

Automating the Inclusion of Subthreshold Signal-to-Noise Ratios for Rapid Gravitational-Wave Localization

Cody Messick,¹ Surabhi Sachdev,^{2,3} Kipp Cannon,⁴ Sarah Caudill,⁵ Chiwai Chan,⁴ Jolien D. E. Creighton,⁶ Ryan Everett,^{2,3} Becca Ewing,^{2,3} Heather Fong,⁴ Patrick Godwin,^{2,3} Chad Hanna,^{2,7,3} Rachael Huxford,^{2,3} Shasvath Kapadia,⁶ Alvin K. Y. Li,⁸ Rico K. L. Lo,^{9,8} Ryan Magee,^{2,3} Duncan Meacher,⁶ Siddharth R. Mohite,⁶ Debnandini Mukherjee,^{2,3} Atsushi Nishizawa,⁴ Hiroaki Ohta,⁴ Alexander Pace,^{2,3} Amit Reza,¹⁰ Minori Shikachi,⁴ Leo Singer,¹¹ Divya Singh,^{2,3} Javed Rana SK,^{2,3} Leo Tsukada,⁴ Daichi Tsuna,⁴ Takuya Tsutsui,⁴ Koh Ueno,⁴ and Aaron Zimmerman¹

¹*The Center for Gravitational Physics, University of Texas, Austin, TX 78712, USA*

²*Department of Physics, The Pennsylvania State University, University Park, PA 16802, USA*

³*Institute for Gravitation and the Cosmos, The Pennsylvania State University, University Park, PA 16802, USA*

⁴*RESCEU, University of Tokyo, Tokyo, 113-0033, Japan*

⁵*Nikhef, Science Park 105, 1098 XG Amsterdam, Netherlands*

⁶*Leonard E. Parker Center for Gravitation, Cosmology, and Astrophysics, University of Wisconsin-Milwaukee, Milwaukee, WI 53201, USA*

⁷*Department of Astronomy & Astrophysics, Pennsylvania State University, University Park, PA, 16802, USA*

⁸*LIGO Laboratory, California Institute of Technology, MS 100-36, Pasadena, California 91125, USA*

⁹*Department of Physics, The Chinese University of Hong Kong, Shatin, New Territories, Hong Kong*

¹⁰*Department of Physics, Indian Institute of Technology Gandhinagar, Gujarat 382355, India*

¹¹*NASA/Goddard Space Flight Center, Greenbelt, MD 20771, USA*

The accurate localization of gravitational-wave (GW) events in low-latency is a crucial element in the search for further multimessenger signals from these cataclysmic events. The localization of these events in low-latency uses signal-to-noise ratio (SNR) time-series from matched-filtered searches which identify candidate events. Here we report on an improvement to the GstLAL-based inspiral pipeline, the low-latency pipeline that identified GW170817 and GW190425, which automates the use of SNRs from all detectors in the network in rapid localization of GW events. This improvement was incorporated into the detection pipeline prior to the recent third observing run of the Advanced LIGO and Advanced Virgo detector network. Previously for this pipeline, manual intervention was required to use SNRs from all detectors if a candidate GW event was below an SNR threshold for any detector in the network. The use of SNRs from subthreshold events can meaningfully decrease the area of the 90% confidence region estimated by rapid localization. To demonstrate this, we present a study of the simulated detections of $\mathcal{O}(2 \times 10^4)$ binary neutron stars using a network mirroring the second observational run of the Advanced LIGO and Virgo detectors. When incorporating subthreshold SNRs in rapid localization, we find that the fraction of events that can be localized down to 100 deg^2 or smaller increases by a factor 1.18.

PACS numbers: 04.80.Nn, 04.25.dg, 95.85.Sz, 97.80.-d 04.30.Db, 04.30.Tv

I. INTRODUCTION

The GstLAL-based inspiral pipeline, referred to as GstLAL in this paper for brevity, is a matched-filtering analysis pipeline designed to search for gravitational waves (GWs) from compact binary inspirals [1–3]. It operates in two modes, low or high latency, and is built using GStreamer, a multimedia streaming framework [4]. The low-latency GstLAL analysis was the first to identify both GW170817 [5] and GW190425 [6], the only two binary neutron star (BNS) mergers confidently identified via GWs to date; it was also the first to identify GW151226 [7], the second confident binary black hole (BBH) merger ever detected. In addition to GstLAL, there are three other low-latency matched-filtering pipelines searching for GWs from compact binary inspirals: PyCBC Live [8], MBTA [9], and SPIIR [10, 11].

One of the primary motivations to search for GWs in low-latency is to enable searches for counterparts by the

global astronomy community. Beginning in Advanced LIGO’s [12] third and Advanced Virgo’s [13] second observing run, O3, any low-latency compact binary merger observation that passed a false alarm rate (FAR) threshold of 1 per 10 months generated a public alert [14]. The preliminary notice, the first public alert generated after the merger [14], for candidates identified by compact binary matched-filter pipelines typically contained a localization estimate produced by BAYESTAR [15]. BAYESTAR estimates the position of the source using a short duration of matched-filter signal-to-noise ratio (SNR) time-series surrounding the time of the candidate from each detector [15]. Information about the candidate is uploaded to the Gravitational-Wave Candidate Event Database (GraceDB) [16], which triggers the BAYESTAR localization [14].

Although the localization performed by BAYESTAR benefits from having all available SNR, GstLAL only considers SNRs above a threshold ρ^* when estimating the

significance of a candidate. Imposing an SNR threshold drastically reduces the number of candidates to consider, hence reducing the computational cost of performing the analysis, while only marginally reducing the sensitivity of the analysis to signals. Prior to O3, acquiring sub-threshold SNRs from GstLAL required manual intervention, meaning the low-latency analysis could not automatically upload all of the SNR available in cases where the maximum SNR in a given detector is below threshold. This was a small effect until the end of O2, when Advanced Virgo joined the observing run with a lower sensitivity than the two advanced LIGO detectors [17]. GW170817 was detected shortly after Virgo joined O2, and although the SNR in Virgo was subthreshold, *i.e.* below ρ^* , the addition of Virgo decreased the 90% confidence region estimated by BAYESTAR from 190 deg² to 31 deg² [5]. Cases like this will become more common as more ground-based detectors of varying sensitivities join the worldwide network of detectors [18], *e.g.* KAGRA [19]. An example of this effect for a simulated BNS signal in simulated Gaussian data can be seen in Fig. 1, the top panel shows the localization estimated by BAYESTAR when only using the advanced LIGO detectors, the middle panel shows the localization when the SNR from Virgo, which is below threshold, is included, and the bottom panel shows the SNR data used in the localization.

GstLAL began providing subthreshold SNRs for rapid localization automatically at the beginning of O3, although they are not used when estimating the significance of candidates. The GStreamer element in the GstLAL pipeline that applies the SNR threshold, referred to as the trigger generator, needed to be redesigned in order to automate the inclusion of subthreshold SNRs. This requirement is specific to GstLAL. PyCBC Live began providing subthreshold SNRs automatically by the end of O2. In this paper, we discuss the redesign of the trigger generator and why it was necessary to automate the inclusion of subthreshold SNRs for rapid localization. We then present the results of a study performed comparing rapid localization of BNS signals using BAYESTAR with and without subthreshold SNRs.

II. AUTOMATING THE INCLUSION OF SUBTHRESHOLD SIGNAL-TO-NOISE RATIOS

GstLAL computes the SNR time-series for each template, or model waveform, and detector at a user-specified rate, typically 2048 Hz, as described in Refs. [1–3, 20]. ‘Triggers’, which consist of a timestamp, an SNR, an autocorrelation-based test-statistic ξ^2 [1, 2], and a template ID, are produced by maximizing the SNR over 1 s windows for each template and computing ξ^2 using the surrounding SNR data from that template and detector [1–3, 20]. If the maximum SNR is less than the user-specified threshold ρ^* , a trigger is not produced. Prior to the work presented here, the SNR data were dis-

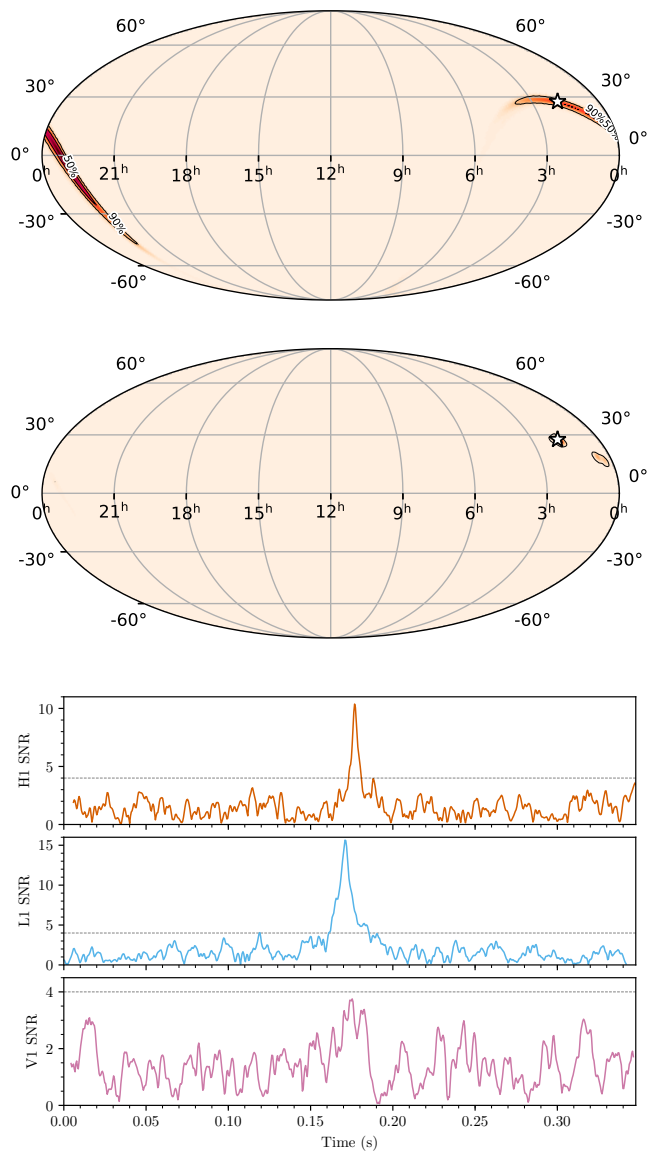


FIG. 1. Top: Localization of a simulated BNS merger estimated by BAYESTAR using only SNR data from detectors that produced SNR peaks above threshold. The star indicates the source of the simulated signal. The total area of the 90% confidence region is 527 deg². Middle: The localization of the same simulated signal, but estimated using SNR from all available detectors. The total area of the 90% confidence region is 85 deg². Bottom: The SNR time-series in each detector made available to use for localization. The dashed line shows the threshold. The network SNR without Virgo is 18.8, with Virgo it is 19.2

carded at this stage for templates that did not produce an SNR peak above threshold, while the SNR data used to compute ξ^2 , typically $\mathcal{O}(100)$ ms, were held in memory for templates that did produce triggers in a given detector. The duration of SNR saved is notably longer than the maximum light-travel-time between detectors and the duration of SNR required by BAYESTAR for

localization. Due to only saving the SNR surrounding a peak above threshold, the only SNR data available to BAYESTAR automatically were from detectors where the maximum SNR in that second was at least as large as ρ^* . In order to obtain the SNR from other detectors that were operating at the time but did not produce an SNR peak above the threshold, the SNR generation stage needed to be manually rerun and configured to write the SNR time-series at a user-provided time to disk before discarding from memory.

The reason that the SNR data were discarded by the trigger generator is that it only considered SNR data from one detector, *i.e.* each detectors' SNR data were ingested by a different instance of the trigger generator and the instances had no knowledge of each other, as seen in the top graphic in Fig. 2. This was an intentional design choice made early in development to avoid the complexity of aggregating multiple time-series streams. However, the GStreamer libraries have undergone many changes since the original design and now include a stable class, `GstAggregator`, that makes synchronizing multiple time-series easier. The new trigger generator is a subclass of `GstAggregator`, and now considers SNR data from all available detectors. If the maximum SNR in a detector is larger than the threshold ρ^* , SNR data surrounding that peak are now saved from all detectors, *e.g.* if an above-threshold peak SNR is identified in the Hanford LIGO detector, SNRs surrounding that time are saved from all available detectors. The duration saved matches the interval used to compute the trigger's ξ^2 test-statistic. The new architecture of the algorithm is depicted in the bottom panel of Fig. 2.

Ingesting multiple time-series required changing several aspects of the trigger generator's algorithm. The internal algorithm that searches for SNR peaks above threshold is unchanged, and is still executed for individual detectors. The primary differences between the original and new trigger generators are: 1) more metadata are saved, *e.g.* the metadata required to retrieve SNR from the other detectors when a peak is identified above threshold; 2) the selection of the interval over which to search for SNR peaks has changed, previously the intervals would bookend gaps and could be different for each detector, but now the same interval is used for all detectors and may include sub-second gaps; and 3) the structure of the buffers output by the element has changed because each output buffer now contains more information than the original trigger generator's output buffers. The last difference also required changes to the elements downstream of the trigger generator in the GstLAL pipeline, *e.g.* new code was written to extract sub-threshold SNR data that were not previously output by the trigger generator.

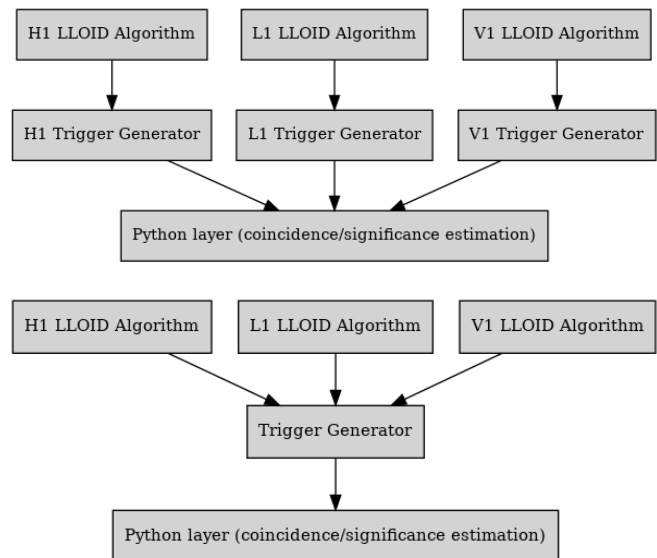


FIG. 2. A view of the old (top) and O3 (bottom) workflows that generate triggers in the GstLAL-based inspiral pipeline. H1, L1, and V1 refer to the Hanford and Livingston LIGO observatories and the Virgo observatory respectively. The LLOID Algorithm [3] computes an SNR time-series at a user-provided rate for each detector, which are then passed to trigger generators that maximize the SNR over 1 s intervals and form a trigger if the maximum passes a user-provided threshold, ρ^* (typically 4). Top: Before O3, a different trigger generator was used for each detector. A small interval of SNR data centered around each trigger were saved by the trigger generator, while the rest were discarded. As a consequence, SNR data from detectors that did not produce a peak above threshold were not automatically available for rapid localization performed by BAYESTAR [15]. Bottom: Beginning in O3, one trigger generator ingests the SNR data from all available detectors. A small interval of SNR data centered around each trigger are now saved by the trigger generator for each detector, *i.e.* if a peak above threshold is identified in one detector then SNR data surrounding the time of that peak are saved from all available detectors. This ensures that rapid localization performed by BAYESTAR in low-latency [14, 15] automatically has access to all available SNR data.

III. INJECTION STUDY

Subthreshold SNRs can be vital in localizing GWs from compact binary mergers. For example, the low SNR of the Virgo trigger associated with GW170817 reduced the area of the 90% confidence region containing the source as estimated by BAYESTAR from 190 deg^2 to 31 deg^2 [5]. Although subthreshold triggers from the GstLAL could be generated in previous observing runs, the manual intervention required added minutes to the latency of producing a localization estimate, a process that can be accomplished in seconds [15].

In order to quantify the effect that subthreshold SNRs have on rapid localization by BAYESTAR, we inserted $\mathcal{O}(2 \times 10^4)$ simulated BNS signals into 13.0 d of simulated

Gaussian data. The Gaussian data were re-colored using public noise curves released by the LIGO Scientific and Virgo Collaborations that are considered representative of the instruments’ sensitivities during O2 [21]. The component masses of the simulated BNS signals are drawn from uniform distributions between $1 M_{\odot}$ and $3 M_{\odot}$, the dimensionless spins are aligned with the binaries’ orbital angular momenta and drawn from uniform distributions from -0.05 to 0.05 , the inclinations are drawn from a uniform distribution, and the distances are drawn from a uniform distribution from 20 Mpc to 800 Mpc. These distributions are not astrophysical, however the distance distribution is expected to generate many signals below an SNR threshold of $\rho^* = 4$ in Virgo given the network sensitivity in O2 [17].

The data with simulated signals were analyzed using the version of GstLAL used to produce the offline significance estimates in Refs. [22–24]. The search was performed using the BNS region of the template bank used in the same searches [22–24], with component masses in the interval $[1, 3) M_{\odot}$ and aligned dimensionless-spin parameters in the interval $[-0.05, 0.05]$. As shown in Fig. 3, the inclusion of subthreshold SNRs decreases the area of the 90% confidence regions for candidates that can be localized down to as low as $\sim 10 \text{ deg}^2$ or as high as $\sim 10^3 \text{ deg}^2$. This can be understood qualitatively as the extremes on either end of the distribution, *i.e.* the signals that can be localized to better than $\sim 10 \text{ deg}^2$ or worse than $\sim 10^3 \text{ deg}^2$, are made up by either extremely loud signals that would not produce subthreshold SNRs or extremely quiet signals that are barely observable. This can further be understood by comparing the area of the 90% confidence regions with and without subthreshold SNRs against the Virgo SNR, as seen in the top panel of Fig. 4. The majority of the decreased area occurs in cases with subthreshold Virgo SNRs; similar behavior is not seen when comparing the sky areas to the SNR in one of the more sensitive LIGO detectors. This is the result of a network of detectors with inhomogeneous sensitivities, which is what we expect for the foreseeable future. Note that the visible gaps around an SNR of 4 in Fig. 4 are due to an artifact in how the peak SNR is computed for peaks below threshold. When a peak is above threshold, GstLAL interpolates the SNR time-series to improve the estimate of SNR, which gives a slight increase in the SNR. This interpolation is not done for the subthreshold case, resulting in a gap just above the threshold ρ^* , but the full SNR time-series is used in the same way to localize the event in both cases. The fraction of candidates localized to 100 deg^2 or smaller increased from $\sim 36\%$ to $\sim 43\%$, an increase of $\sim 18\%$ relative to the rate without subthreshold SNRs.

IV. CONCLUSION

We presented work performed to automate the inclusion of subthreshold SNRs into GraceDB [16] uploads

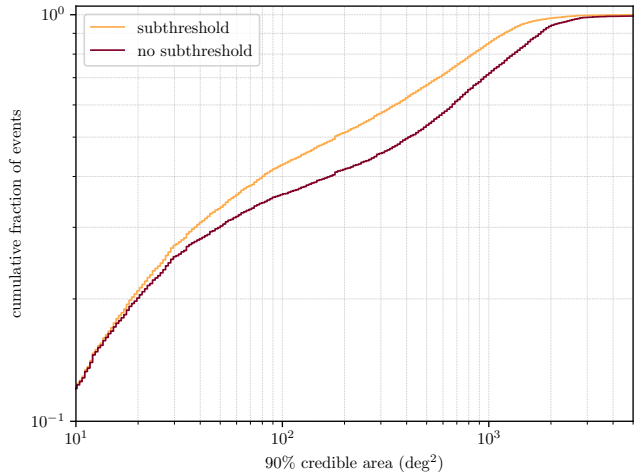


FIG. 3. The fractional cumulative number of events localized to a 90% credible region as a function of the 90% credible region area. The events here are $\mathcal{O}(2 \times 10^4)$ fake BNS signals injected into 13.0 days of Gaussian data that were re-colored using publicly available noise curves that represent the sensitivity of the Advanced LIGO and Advanced Virgo detectors during O2. The line labeled “subthreshold” shows the cumulative number of events when including subthreshold SNRs in the localization calculation performed by BAYESTAR [15], while the line labeled “no subthreshold” shows the cumulative number of events when subthreshold SNRs are not used by BAYESTAR. Prior to the work presented here, inclusion of subthreshold SNRs when localizing candidates identified by the GstLAL-based inspiral pipeline required manual intervention which added $\mathcal{O}(\text{minutes})$ of latency to a process that can take only seconds [15]. The cumulative fraction of events that are localized to a region smaller than 100 deg^2 increased from $\sim 36\%$ to $\sim 43\%$ upon the inclusion of SNRs.

for use in localization by BAYESTAR [15]. The original and current workflows that generate triggers and dictate what SNRs are preserved in GstLAL are shown in Fig. 2, and a study comparing the localization with and without subthreshold SNRs is shown in Fig. 3. The rate at which candidates were localized to 100 deg^2 or less increased from $\sim 36\%$ to $\sim 43\%$. The new trigger generator described here was used by GstLAL for the entirety of O3.

ACKNOWLEDGMENTS

We gratefully acknowledge the support of the Eberly Research Funds of Penn State and the National Science Foundation through OAC-1841480, PHY-1454389, and PHY-1912578. The authors are grateful for computational resources provided by the LIGO Lab and supported by the National Science Foundation through PHY-1626190 and PHY-1700765. This document has LIGO document number: P2000445.

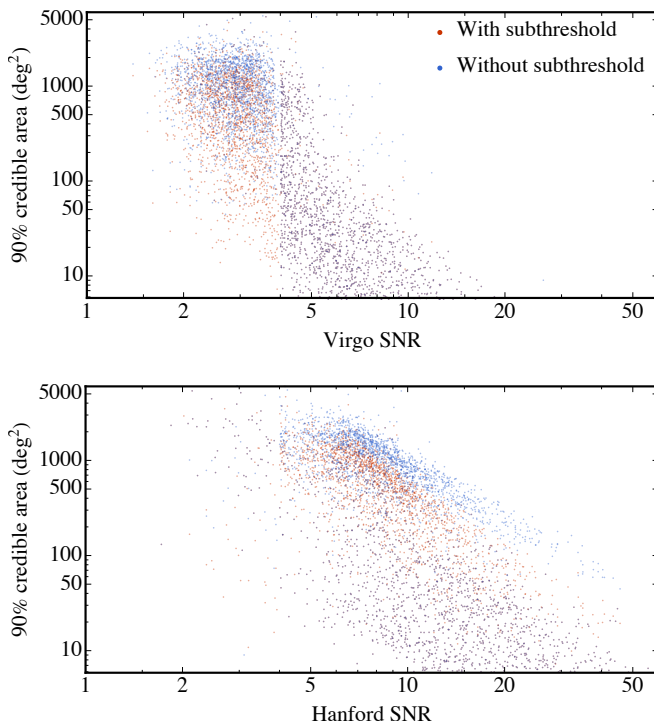


FIG. 4. Scatter plots of the 90% confidence areas estimated by BAYESTAR for the recovered simulated BNS signals. Top: The areas compared to the SNR in Virgo. The SNR threshold used for this search was $\rho^* = 4$. A clear improvement in area is observed for Virgo triggers below threshold, which is the expected behavior given the relative detector sensitivities. Bottom: The areas compared to the SNR in the Hanford, WA LIGO detector for comparison to the top panel.

-
- [1] S. Sachdev, S. Caudill, H. Fong, R. K. Lo, C. Messick, D. Mukherjee, R. Magee, L. Tsukada, K. Blackburn, P. Brady, *et al.*, arXiv preprint arXiv:1901.08580 (2019).
- [2] C. Messick, K. Blackburn, P. Brady, P. Brockill, K. Cannon, R. Cariou, S. Caudill, S. J. Chamberlin, J. D. Creighton, R. Everett, *et al.*, Physical Review D **95**, 042001 (2017).
- [3] K. Cannon, R. Cariou, A. Chapman, M. Crispin-Ortuzar, N. Fotopoulos, M. Frei, C. Hanna, E. Kara, D. Koppel, L. Liao, *et al.*, The Astrophysical Journal **748**, 136 (2012).
- [4] G. Team, “Gstreamer: open source multimedia framework,” (2020).
- [5] B. P. Abbott, R. Abbott, T. Abbott, F. Acernese, K. Ackley, C. Adams, T. Adams, P. Addesso, R. Adhikari, V. Adya, *et al.*, Physical Review Letters **119**, 161101 (2017).
- [6] B. Abbott, R. Abbott, T. Abbott, S. Abraham, F. Acernese, K. Ackley, C. Adams, R. Adhikari, V. Adya, C. Affeldt, *et al.*, The Astrophysical Journal Letters **892**, L3 (2020).
- [7] B. P. Abbott, R. Abbott, T. Abbott, M. Abernathy, F. Acernese, K. Ackley, C. Adams, T. Adams, P. Addesso, R. Adhikari, *et al.*, Physical review letters **116**, 241103 (2016).
- [8] A. H. Nitz, T. Dal Canton, D. Davis, and S. Reyes, Physical Review D **98**, 024050 (2018).
- [9] T. Adams, D. Buskulic, V. Germain, G. M. Guidi, F. Marion, M. Montani, B. Mours, F. Piergiovanni, and G. Wang, Classical and Quantum Gravity **33**, 175012 (2016).
- [10] S. Hooper, S. K. Chung, J. Luan, D. Blair, Y. Chen, and L. Wen, Physical Review D **86**, 024012 (2012).
- [11] Q. Chu, PhDT (2017).
- [12] J. Aasi, B. Abbott, R. Abbott, T. Abbott, M. Abernathy, K. Ackley, C. Adams, T. Adams, P. Addesso, R. Adhikari, *et al.*, Classical and quantum gravity **32**, 074001 (2015).
- [13] F. Acernese, M. Agathos, K. Agatsuma, D. Aisa, N. Allemandou, A. Allocca, J. Amarni, P. Astone, G. Balestri, G. Ballardín, *et al.*, Classical and Quantum Gravity **32**, 024001 (2014).
- [14] LIGO Scientific Collaboration, Virgo Collaboration, **Public Alerts User Guide (2019)**.
- [15] L. P. Singer and L. R. Price, Physical Review D **93**, 024013 (2016).
- [16] “Gravitational-wave candidate event database,” <https://gracedb.ligo.org>, accessed: 2019-06-04.

- [17] L. S. Collaboration, V. Collaboration, *et al.*, arXiv preprint arXiv:1811.12907 (2018).
- [18] B. Abbott *et al.* (KAGRA, LIGO Scientific, VIRGO), *Living Rev. Rel.* **21**, 3 (2018), arXiv:1304.0670 [gr-qc].
- [19] T. Akutsu, M. Ando, K. Arai, Y. Arai, S. Araki, A. Araya, N. Aritomi, Y. Aso, S.-W. Bae, Y.-B. Bae, *et al.*, arXiv preprint arXiv:2005.05574 (2020).
- [20] K. Cannon, A. Chapman, C. Hanna, D. Keppel, A. C. Searle, and A. J. Weinstein, *Physical Review D* **82**, 044025 (2010).
- [21] “Ligo document p1800374-v1,” <https://dcc.ligo.org/P1800374/public/>, accessed: 2020-10-26.
- [22] L. S. Collaboration, V. Collaboration, *et al.*, arXiv preprint arXiv:2004.08342 (2020).
- [23] R. Abbott, T. Abbott, S. Abraham, F. Acernese, K. Ackley, C. Adams, R. Adhikari, V. Adya, C. Affeldt, M. Agathos, *et al.*, *Physical review letters* **125**, 101102 (2020).
- [24] R. Abbott, T. Abbott, S. Abraham, F. Acernese, K. Ackley, C. Adams, R. Adhikari, V. Adya, C. Affeldt, M. Agathos, *et al.*, *The Astrophysical Journal Letters* **896**, L44 (2020).